


Cite this: *RSC Adv.*, 2018, 8, 6581

Fabrication of a hyaluronic acid conjugated metal organic framework for targeted drug delivery and magnetic resonance imaging

Fangpeng Shu,^a Daojun Lv,^a Xian-Lu Song,^b Bin Huang,^a Chong Wang,^a Yuzhong Yu^a and Shan-Chao Zhao ^{*a}

Since metal organic frameworks (MOF) have exhibited fascinating potential in biomedical applications, it is worthwhile to construct a MOF-based multifunctional drug delivery system. In the present study, the anticancer drug doxorubicin (DOX) was loaded into zeolitic imidazolate framework-8 (ZIF-8) via a one-pot process. The formed DOX@ZIF-8 was then coated with polydopamine, successively chelated with Fe³⁺ and conjugated with hyaluronic acid (HA), finally resulting in a multifunctional ZIF-8 nanocarrier. The characterization results confirmed the successful formation of the hybrid nanocarrier. pH-responsive drug release of DOX was observed due to the innate pH-dependent stability of ZIF-8. Importantly, the flow cytometry and confocal laser scanning microscope results both verified the targeting ability of DOX@ZIF-HA toward prostate cancer PC-3 cells. The improved therapeutic efficacy of DOX@ZIF-HA when compared to the inhibited group was also demonstrated. Furthermore, the chelation of Fe³⁺ by PDA makes the prepared DOX@ZIF-HA a good contrast agent for magnetic resonance (MR) imaging. Hence, we hope the constructed ZIF-8 based multifunctional nanocarrier could be a candidate for cancer theranostics.

Received 1st December 2017
Accepted 26th January 2018

DOI: 10.1039/c7ra12969f

rsc.li/rsc-advances

1. Introduction

As one of the most frequently used approaches for combating cancer, chemotherapy has always suffered some unbearable drawbacks, including non-specific toxicity toward normal cells, premature degradation in circulation and insufficient therapeutic efficacy.¹ To address those problems, various nanocarriers, such as liposomes,² polymer micelles,³ graphene⁴ and mesoporous silica nanoparticles,⁵ have been widely developed for packaging and delivering chemotherapeutic drugs. Nanocarriers can not only protect the drug from rapid clearance, but can also improve its accumulation at the tumor site through the enhanced permeability and retention (EPR) effect.⁶ However, currently explored nanocarriers still have a few shortcomings to conquer. For instance, the stability of organic nanocarriers is poor and they can only offer single functionality,⁷ while debates about the biocompatibility and biodegradability of inorganic nanocarriers have never stopped.⁸ The construction of organic/inorganic hybrid nanocarriers could adequately integrate the functionality of inorganic nanomaterials with the biocompatibility of organic nanomaterials.⁹ Unfortunately, simple hybridization still fails to change their innate physiochemical

properties. As a consequence, the development of novel nanocarriers with a natural organic/inorganic constitution may strongly promote the translation process of nanomedicine.

Metal organic frameworks (MOFs) are highly porous materials composed of metal ions and organic linkers.¹⁰ In particular, nano-scale MOFs have drawn extensive attention owing to their high surface area, tunable shapes and pore sizes, and controllable surface functionalities.¹¹ Built from zinc ions and imidazole units, zeolitic imidazolate framework-8 (ZIF-8) is one of the most widely investigated subclasses of MOFs for biomedical applications.¹² It is well known that ZIF-8 can decompose under lower pH conditions,¹³ thus making it a good candidate for a pH-responsive nanocarrier for drug delivery. For instance, Wang's group¹⁴ developed a facile two-step method to fabricate green fluorescent carbon nanodots@ZIF-8 with adjustable size and fluorescence intensity, then the prepared hybrid ZIF-8 was loaded with 5-fluorouracil and a pH-responsive drug release behavior was demonstrated. In another study, He *et al.*¹⁵ prepared CuS-encapsulated ZIF-8 and then the anti-cancer drug doxorubicin (DOX) was loaded into the hybrid ZIF-8 nanoparticles for combined therapy. However, the drug loading process in those studies was mostly accomplished in two steps: the formation of ZIF-8 and the absorption of the drug. This approach always suffers from low loading efficacy and poorly controlled release of the molecules. Very recently, Zou and co-workers¹⁶ proposed a one-pot synthetic procedure for the preparation of targeted molecule-encapsulated ZIF-8 in the

^aDepartment of Urology, Nanfang Hospital, Southern Medical University, Guangzhou 510515, China. E-mail: zhaoshanchaosu@sina.cn

^bDepartment of Radiation Oncology, Affiliated Cancer Hospital & Institute of Guangzhou Medical University, Guangzhou 510095, China



constructed multifunctional nanocarrier possessed both therapeutic and diagnostic functions.

2. Experimental section

Zn(NO₂)₃·6H₂O, 2-methylimidazole, dopamine hydrochloride and FeCl₃·6H₂O were purchased from Sigma-Aldrich Trading Co., Ltd. Amino-poly(ethylene glycol) (PEG-NH₂, *M_w* ~ 2000 Da) was received from JenKem Technology Co, Ltd. Doxorubicin hydrochloride was bought from Beijing Huafeng United Technology Co., Ltd. Roswell Park Memorial Institute (RPMI) 1640 medium, trypsin, fetal bovine serum (FBS) and penicillin-streptomycin solution were supplied by Hyclone (Thermo Scientific, USA). A cell counting kit-8 (CCK-8) was provided by Sigma-Aldrich Trading Co., Ltd. 4',6-Diamidino-2-phenylindole (DAPI) was received from Vector laboratories (Burlingame, CA). All other reagents were of analytical grade and used without further purification. Deionized (DI) water was used throughout all experiments.

Chemotherapeutic DOX was incorporated into the framework of ZIF-8 *via* a “one-pot” method.¹⁶ Generally, DOX was dissolved in DI water at 4 mg mL⁻¹. Then 0.2 g (0.66 mmol) of Zn(NO₃)₂·6H₂O was dissolved in 0.8 mL water, into which 4 mL of DOX solution was added and vigorously stirred for 1 min. After that 2 g 2-methylimidazole was dissolved in 8 mL water and this was slowly dropped into the mixture. The reaction was maintained at room temperature for 15 min. The DOX@ZIF-8 nanoparticles were collected using high-speed centrifugation and washed with DI water three times.

To modify their inert surface, polydopamine (PDA) was coated onto DOX@ZIF-8 *via* mussel-inspired polymerization.²⁴ Briefly, 20 mg DOX@ZIF-8 was ultrasonically dispersed in 20 mL Tris-HCl solution (pH 8.5, 10 mM). Then 10 mg dopamine hydrochloride was added and the reaction was continued for 4 h. PDA-coated DOX@ZIF-8 was separated by centrifugation and washed with DI water.

The target molecule HA was conjugated onto DOX@ZIF-8 *via* an Fe³⁺-mediated coordination reaction.²⁵ Typically, 10 mg DOX@ZIF-PDA was dispersed in 10 mL Tris-HCl solution (pH 8.5, 10 mM). Then 0.1 mL of FeCl₃ solution was added and stirred for 1 h. Subsequently, 10 mg HA was introduced into the mixture and stirred for another 3 h. Finally, the hybrid nanoparticles were collected by centrifugation and repeatedly washed. The HA modified DOX@ZIF-8 was denoted DOX@ZIF-HA.

This journal is © The Royal Society of Chemistry 2018



Fig. 1 A schematic diagram for the preparation of DOX@ZIF-HA and the Fe^{3+} -mediated coordination interaction between HA and PDA.

PDA, onto which an Fe ion was chelated and HA was conjugated to obtain DOX@ZIF-HA. The prepared MOF, before and after functionalization, was explored by TEM. As presented in Fig. 2B, we successfully fabricated nano-scale DOX@ZIF-8, which clearly displayed a spherical appearance with a diameter of around 150 nm. In contrast, the bare ZIF-8 nanoparticles without DOX loading showed a typical hexagonal structure (Fig. 2A). After functionalization, the TEM images suggest that a more rough surface could be observed (Fig. 2C and D), whereas no

significant change was observed in the morphology of the obtained nanoparticles when compared to pristine DOX@ZIF-8. To further confirm this, an FESEM image of DOX@ZIF-HA is presented in Fig. 2E. It can be easily seen that DOX@ZIF-HA still maintained a round shape and no apparent particle agglomeration occurred, which is beneficial for its application in drug delivery. The crystal phase was also monitored by XRD. As shown in Fig. 2F, pristine DOX@ZIF-8 exhibited well-defined diffraction peaks that correspond to the high crystallinity of



Fig. 2 TEM images of (A) pure ZIF-8, (B) DOX@ZIF-8, (C) DOX@ZIF-PDA and (D) DOX@ZIF-HA nanoparticles. (E) An FESEM image of the prepared DOX@ZIF-HA. (F) The XRD results of the prepared nanoparticles.



ZIF-8.²⁶ Those characteristic peaks were still retained after functionalization was completed, however, a weak broad peak emerged around 20°, which could be assigned to the organic shell.²⁷

Since a good colloidal stability of nanocarriers is a prerequisite for their application, we next inspected the colloidal stability of the as-synthesized DOX@ZIF-HA in different media. DLS was applied to measure the size distribution of those dispersions (Fig. 3A). It was found that the size distribution of DOX@ZIF-HA in PBS and cell culture medium was similar to that in DI water, somewhat reflecting that no agglomeration happened even when DOX@ZIF-HA was dispersed in a solution with a high ionic strength. It was also noticed that the size of DOX@ZIF-HA was slightly increased in FBS, which might be ascribed to the nonspecific adsorbed protein on its surface.²⁸ Meanwhile, the dispersions were stored under ambient conditions for 12 h, and the obtained photograph indicated that no large particles appeared in the dispersions (Fig. 3B), further confirming the colloidal stability of DOX@ZIF-HA in different media.

Zeta potential measurements were performed to detect the surface charge of the prepared nanoparticles. Fig. 4A demonstrates that the as-synthesized DOX@ZIF-8 displayed a positively-charged surface with a zeta potential of 27.1 mV, while PDA modification gives the hybrid nanoparticles a negatively-charged surface owing to the abundant phenolic groups of PDA.²⁹ After the attachment of acid mucopolysaccharide HA,³⁰ the obtained DOX@ZIF-HA still maintained a highly negative potential with a value of −30.2 mV. Logically, the higher negative potential could ensure good colloidal stability of the nanomaterials under physiological conditions,³¹ resulting in good colloidal stability of DOX@ZIF-HA as illustrated above. Afterwards, the chemical composition of the prepared nanoparticles was also investigated using FTIR. As depicted in Fig. 4B, the spectrum of pure ZIF-8 appeared to be typical, and the 1574 and 1145 cm^{−1} bands belong to C=N stretching vibrations. Moreover, the strong peak at 1077 cm^{−1}, assigned to the C-N stretching of the imidazole units, was observed in both pure ZIF-8 and the other nanoformulations.³² Obviously, the bands in the range of 2800–3200 cm^{−1} resulted from C-H vibrations in the backbone ring structure.³³ A new peak at

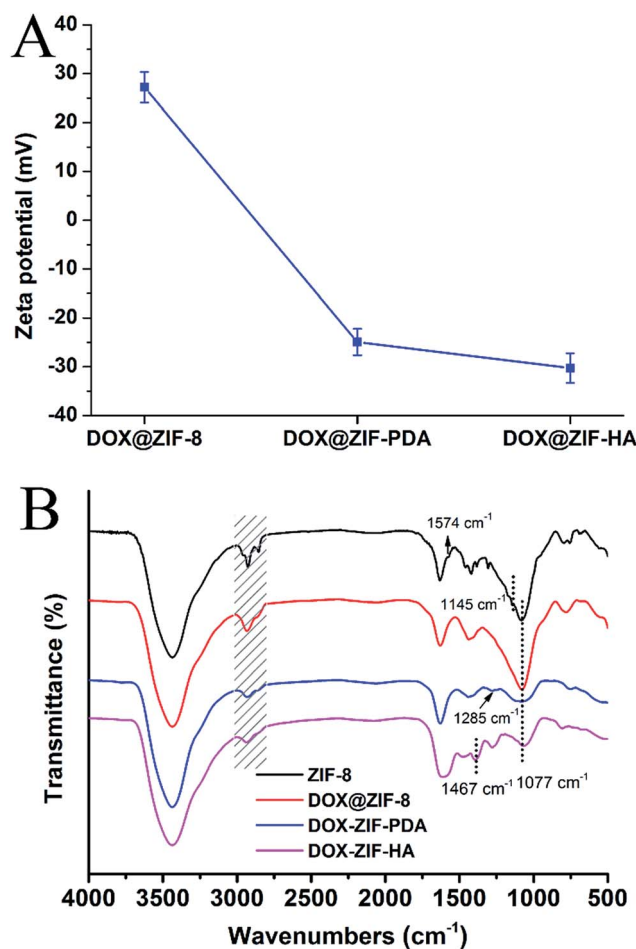


Fig. 4 (A) Surface zeta potential and (B) FTIR spectra of the prepared nanoparticles in different stages.

1285 cm^{−1}, corresponding to the C-O vibration from the phenolic hydroxyl group, was clearly observed after the modification with PDA,³⁴ and the sharp peak at 1077 cm^{−1} was weakened and broadened at the same time. Besides, the typical absorption peaks of the amide bond were also detected in the spectrum of DOX@ZIF-HA because of the *N*-acetylglucosamine of HA. Specifically, three adjacent peaks at 1610, 1476 and



Fig. 3 (A) The size distribution of DOX@ZIF-HA dispersed in different media, as measured by DLS. (B) Photographs of different DOX@ZIF-HA dispersions stored under ambient conditions for 1 h and 12 h.



1394 cm^{-1} were attributed to the absorption of the amide I, II and III bands,³⁵ respectively. When combined with the above discussion, it can be concluded that the designed hybrid nanoplateform was successfully fabricated.

3.2. Drug release property

After the successful construction of DOX@ZIF-HA was verified, the release behavior of the incorporated DOX was successively investigated. The loading efficacy was determined to be $8.92 \pm 0.53\%$. Fig. 5 shows the release kinetics of DOX from DOX@ZIF-HA under different pH conditions. The data suggest that the release of DOX from the nanocarrier demonstrated a sustained nature regardless of the pH condition. In particular, a pH-dependent drug release behavior was observed. It can be seen that 34% of DOX was released from DOX@ZIF-HA in the first 6 h under acidic conditions (pH 5.0), while the released amount of DOX was only 7.7% under physiological pH conditions over the same time period. At the end, the cumulative amount of DOX released at pH 5.0 and 7.4 was 70.1% and 9.8%, respectively. The pH-dependent release behavior is reasonable owing to the dissolution mechanism of the nanoscale ZIF-8 structure. It has been widely demonstrated that the coordination interaction between Zn^{2+} and imidazole would be disrupted under lower pH conditions,³⁶ which then encourages the locked DOX to diffuse out. Another potential reason lies in the better hydrophilicity of DOX under acidic conditions, when compared to that under neutral conditions.³⁷ Anyway, there is no doubt that the rapid release of DOX at pH 5.0 could dramatically improve the delivery efficacy considering the more acidic tumor microenvironment when compared to that of normal tissues.

3.3. Targeted cellular uptake

Apart from the stimuli-responsive drug release properties, the targeted drug delivery could further enhance the chemotherapeutic efficacy.³⁸ The targeting ability of DOX@ZIF-HA toward the prostate cancer cell line PC-3 was first evaluated by flow cytometry. The PC-3 cells were treated with different

concentrations of DOX@ZIF-HA for 2 h and then subjected to the FCM test. The cells incubated with PBS were used as a control and the cells pre-treated with free HA were used for comparison. The data demonstrated that the intracellular fluorescence intensity was distinctly improved with the increase of DOX@ZIF-HA concentration (Fig. 6A). It is worth noting that the mean fluorescence of cells pre-treated with free HA was higher than that of cells directly treated with DOX@ZIF-HA at the same concentration. Specifically, the value decreased from 217.37 to 193.19 at a concentration of $100 \mu\text{g mL}^{-1}$ after pre-treatment with free HA (Fig. 6B). Considering the widely reported overexpressed CD44 receptor on PC-3 cells,^{39,40} the value decrease was because the free HA would inhibit the overexpressed CD44 receptor on PC-3 cells. Thus, it can be deduced that the prepared DOX@ZIF-HA could efficiently target PC-3 cells.

Moreover, the cells were incubated with free DOX and DOX@ZIF-HA for 2 h and CLSM was applied to visually observe their intracellular uptake. As presented in Fig. 7A, the red fluorescence of DOX completely overlapped with the blue fluorescence of the DAPI-stained cell nucleus, while the red spot of DOX@ZIF-HA was mainly distributed in the cell cytoplasm and localized around the cell nucleus. As a small molecule drug,



Fig. 5 The cumulative release curve of DOX@ZIF-HA under different pH conditions.



Fig. 6 (A) Flow cytometric analysis of HeLa cells treated with different concentrations of DOX@ZIF-HA for 2 h, free HA was used to inhibit CD44 receptors on PC-3 cells for comparison. (B) Mean fluorescence density in PC-3 cells after the corresponding treatment (* for $p < 0.05$ and ** for $p < 0.01$).





Fig. 7 CLSM images of (A) PC-3 cells and (B) L929 cells, treated with free DOX and DOX@ZIF-HA for 2 h, the cells pre-treated with HA were observed for comparison. The blue and red fluorescence represents the DAPI-stained cell nucleus and DOX, respectively.

DOX entered into PC-3 cells *via* passive diffusion, thus resulting in rapid entrance into the cell nucleus. In contrast, the nano-carrier was actively transported into the cell interior by enclosing it in vesicles.⁴¹ So the retention of DOX@ZIF-HA in the cytoplasm could facilitate the sustained release of DOX and maintain a sufficient drug concentration in cancer cells.⁴² In addition, the enhanced uptake of DOX@ZIF-HA by the PC-3 cells was also confirmed. It can be seen that the fluorescence in the case of DOX@ZIF-HA was much stronger than that of the cells pre-treated with free HA. This result should be attributed to the inhibition of the overexpressed CD44 receptors on the PC-3 cell surface by free HA, leading to the subdued targeting ability of DOX@ZIF-HA.

Normal cells L929 were also employed to further confirm the targeting ability of DOX@ZIF-HA toward specific cancer cells. As seen in Fig. 7B, the free DOX also directly diffused into the cell nucleus. Meanwhile, it also can be observed that red spots of DOX@ZIF-HA accumulated in the cytoplasm. Notably, the fluorescence intensity of L929 cells was clearly lower than that of PC-3 cells. This tendency could probably be attributed to the negative surface of DOX@ZIF-HA. Meanwhile, it is worth noting that the treatment of free HA didn't reduce the internalization of DOX@ZIF-HA, showing the different uptake behavior with CD44-overexpressed PC-3 cells. Predictably, the targeting ability of DOX@ZIF-HA would lose its "magic" toward a normal cell line due to the lower expression of the CD44 receptor on L929. Taken together, the above results forcefully affirm that DOX@ZIF-HA could efficiently enhance intracellular uptake and deliver more of the drug into PC-3 cells.

3.4. *In vitro* killing efficacy of PC-3 cells

After confirming the targeting ability of DOX@ZIF-HA, its therapeutic activity against PC-3 cells was assessed using the

CCK-8 assay. The cells were treated with different formulations for 24 h and un-treated cells were used as a control. As shown in Fig. 8A, the viability of treated PC-3 cells clearly decreased with increased DOX concentration. Specifically, the toxicity of DOX@ZIF-HA was significantly higher than that of free DOX at the same concentration. For instance, at a DOX concentration of $1 \mu\text{g mL}^{-1}$, the cell viability for free DOX and DOX@ZIF-HA was 65.61% and 48.59%, respectively. This is mainly due to the fact that the efficient internalization of the targeted carrier DOX@ZIF-HA could improve the intracellular DOX concentration.⁴³ Furthermore, the inhibition assay was also performed to demonstrate the targeting ability. It was observed that the toxicity of DOX@ZIF-HA clearly decreased in the presence of free HA. In particular, the cell viability of DOX@ZIF-HA was 20.22% at a DOX concentration of $4 \mu\text{g mL}^{-1}$, while the value increased to 26.56% after pre-treatment with free HA. Undoubtedly, the decrease in therapeutic efficacy was caused by the inhibition of free HA toward the targeting ability of DOX@ZIF-HA. To further demonstrate the discrepancy, live cell staining was performed. Fig. 8C shows the fluorescent imaging of PC-3 cells treated with different formulations. It can be seen that the strong green fluorescence was overspread on the culture well for the control group, while the amount of live cells sharply decreased after incubation with different treatments. In particular, DOX@ZIF-HA treated cells exhibited a higher mortality rate as compared to free DOX-treated PC-3 cells and the inhibited group, suggesting the same tendency as the quantitative results.

For comparison, L929 cells were also subjected to the same treatments and the data are presented in Fig. 8B. Although the cell viabilities decreased with elevated DOX concentrations, it should be noted that the survival rate of L929 cells was distinctly lower than that of PC-3 cells at an equivalent DOX





Fig. 8 The CCK-8 assay of (A) PC-3 cells and (B) L929 cells, treated with free DOX and DOX@ZIF-HA at different DOX concentrations for 24 h. (C) Live cell staining (Calcein-AM) of PC-3 cells treated with (C₁) culture medium, (C₂) free DOX, (C₃) DOX@ZIF-HA plus free HA and (C₄) DOX@ZIF-HA, at a DOX concentration of 4 µg mL⁻¹.

concentration. Not surprisingly, the inhibition of free HA exerted negligible influence on the therapeutic efficacy of DOX@ZIF-HA. Specifically, at a DOX concentration of 4 µg mL⁻¹, the viability for free DOX, DOX@ZIF-HA and DOX@ZIF-HA plus free HA treated L929 cells was 45.04%, 39.84% and 43.56%, respectively. It could be expected that the lower toxicity of DOX@ZIF-HA against L929 would alleviate its side effects toward normal organs, somewhat highlighting the intrinsic merit of actively targeted nanocarriers. Therefore, the above results suggest that the prepared DOX@ZIF-HA could be efficiently applied as an actively targeted nanocarrier to improve chemotherapeutic efficacy.

3.5. *In vitro* MR imaging ability

Apart from mediating the conjugation of HA, the chelation of Fe³⁺ by PDA could also be used as a T₁ contrast agent.^{44,45} So the MR imaging ability of DOX@ZIF-HA was evaluated *in vitro*. As expected, the longitudinal relaxation time (T₁) decreased correlatively with increased Fe concentration (Fig. 9). The r₁ value was calculated to be 5.57 mM⁻¹ s⁻¹, which is higher than a clinically used MRI contrast agent Gd-DTPA. Correspondingly, the MR images of DOX@ZIF-HA dispersions became brighter with the increase of Fe concentration (inset photos in Fig. 9), implying their favorable MR imaging ability. Thus, the DOX@ZIF-HA could also act as an excellent contrast agent for MR imaging.

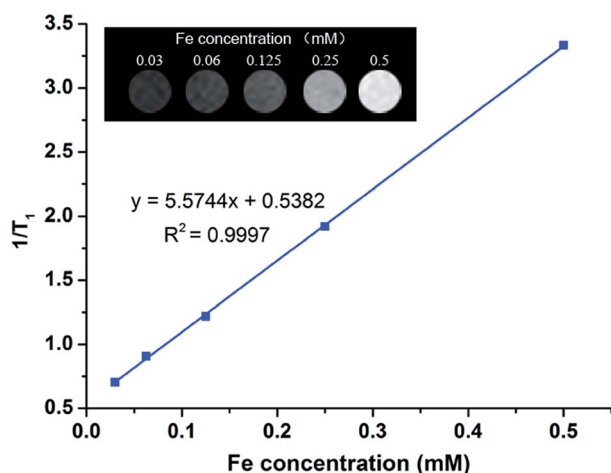


Fig. 9 The *in vitro* MR imaging ability of DOX@ZIF-HA. The linear fitting of 1/T₁ as a function of Fe concentration. The inset pictures represent the corresponding T₁-weighted MR images of DOX@ZIF-HA at different Fe concentrations.

4. Conclusion

In summary, DOX-doped MOF nanoparticles were prepared *via* a one-pot reaction and successively anchored with Fe³⁺ and HA for simultaneous targeted drug delivery and MR imaging. The successful construction of DOX@ZIF-HA was confirmed by a series of physicochemical characterization techniques. The incorporated DOX could be released from the nanocarrier in a sustained and pH-sensitive manner. The inhibition experiment also demonstrated that the targeting ability of DOX@ZIF-8-HA toward CD44 overexpressed PC-3 cells could efficiently improve its intracellular uptake and further enhance the *in vitro* chemotherapeutic efficacy as compared to free DOX. Moreover, the chelation of Fe³⁺ endowed DOX@ZIF-HA with a favorable contrast ability for MR imaging. Overall, the developed DOX@ZIF-HA could be applied as a potential theranostic agent for chemotherapy of CD44 overexpressed PC-3 cells and MR imaging.



Conflicts of interest

There are no conflicts to declare.

Acknowledgements

This study was supported by three Science and Technology planning Projects of Guangdong Province (No. 2013B051000050, No. 2014A020212538 and No. 2016A020215175), the Natural Science Foundation of Guangdong Province (No. 2016A030313583), the Medical Scientific Research Foundation of Guangdong Province (No. A2016555), the Science and Technology planning Project of Guangzhou (No. 201704020070), and the Outstanding Youths Development Scheme of Nanfang Hospital, Southern Medical University (No. 2015J005).

References

- 1 P. Couvreur, *Adv. Drug Delivery Rev.*, 2013, **65**, 21–23.
- 2 C. Yao, P. Wang, X. Li, X. Hu, J. Hou, L. Wang and F. Zhang, *Adv. Mater.*, 2016, **28**, 9341–9348.
- 3 V. G. Deepagan, S. Kwon, D. G. You, V. Q. Nguyen, W. Um, H. Ko, H. Lee, D. G. Jo, Y. M. Kang and J. H. Park, *Biomaterials*, 2016, **103**, 56–66.
- 4 K. Yang, L. Feng and Z. Liu, *Adv. Drug Delivery Rev.*, 2016, **105**, 228–241.
- 5 J. Wen, K. Yang, F. Liu, H. Li, Y. Xu and S. Sun, *Chem. Soc. Rev.*, 2017, **46**, 6024–6045.
- 6 W. Cui, J. Li and G. Decher, *Adv. Mater.*, 2016, **28**, 1302–1311.
- 7 Y. Chen and J. Shi, *Adv. Mater.*, 2016, **28**, 3235–3272.
- 8 E. B. Ehlerding, F. Chen and W. Cai, *Adv. Sci.*, 2016, **3**, 1600122.
- 9 P. Huang, Y. Chen, H. Lin, L. Yu, L. Zhang, L. Wang, Y. Zhu and J. Shi, *Biomaterials*, 2017, **125**, 23–37.
- 10 D. MasPOCH, D. Ruiz-Molina and J. Veciana, *Chem. Soc. Rev.*, 2007, **36**, 770–818.
- 11 J. Della Rocca, D. Liu and W. Lin, *Acc. Chem. Res.*, 2011, **44**, 957–968.
- 12 W. Cai, C. C. Chu, G. Liu and Y. X. Wang, *Small*, 2015, **11**, 4806–4822.
- 13 C. Y. Sun, C. Qin, X. L. Wang, G. S. Yang, K. Z. Shao, Y. Q. Lan, Z. M. Su, P. Huang, C. G. Wang and E. B. Wang, *Dalton Trans.*, 2012, **41**, 6906–6909.
- 14 L. He, T. T. Wang, J. P. An, X. M. Li, L. Y. Zhang, L. Li, G. Z. Li, X. T. Wu, Z. M. Su and C. G. Wang, *CrystEngComm*, 2014, **16**, 3259–3263.
- 15 Z. F. Wang, X. J. Tang, X. X. Wang, D. D. Yang, C. Yang, Y. B. Lou, J. X. Chen and N. Y. He, *Chem. Commun.*, 2016, **52**, 12210–12213.
- 16 H. Q. Zheng, Y. N. Zhang, L. F. Liu, W. Wan, P. Guo, A. M. Nystrom and X. D. Zou, *J. Am. Chem. Soc.*, 2016, **138**, 962–968.
- 17 M. Zheng, S. Liu, X. G. Guan and Z. G. Xie, *ACS Appl. Mater. Interfaces*, 2015, **7**, 22181–22187.
- 18 Q. Chen and Z. Liu, *Adv. Mater.*, 2016, **28**, 10557–10566.
- 19 A. R. Chowdhuri, D. Laha, S. Pal, P. Karmakar and S. K. Sahu, *Dalton Trans.*, 2016, **45**, 18120–18132.
- 20 R. X. Bian, T. T. Wang, L. Y. Zhang, L. Li and C. G. Wang, *Biomater. Sci.*, 2015, **3**, 1270–1278.
- 21 F. Ravar, E. Saadat, M. Gholami, P. Dehghankelishadi, M. Mahdavi, S. Azami and F. A. Dorkoosh, *J. Controlled Release*, 2016, **229**, 10–22.
- 22 Q. Zhao, S. Wang, Y. Yang, X. Li, D. Di, C. Zhang, T. Jiang and S. Wang, *Mater. Sci. Eng., C*, 2017, **78**, 475–484.
- 23 D. D. Gurav, A. S. Kulkarni, A. Khan and V. S. Shinde, *Colloids Surf., B*, 2016, **143**, 352–358.
- 24 H. Lee, S. M. Dellatore, W. M. Miller and P. B. Messersmith, *Science*, 2007, **318**, 426–430.
- 25 J. Han, W. Park, S. J. Park and K. Na, *ACS Appl. Mater. Interfaces*, 2016, **8**, 7739–7747.
- 26 H. P. Jing, C. C. Wang, Y. W. Zhang, P. Wang and R. Li, *RSC Adv.*, 2014, **4**, 54454–54462.
- 27 B. Q. Mao, Q. D. An, B. Zhai, Z. Y. Xiao and S. R. Zhai, *RSC Adv.*, 2016, **6**, 47761–47770.
- 28 Y. S. Lin, N. Abadeer and C. L. Haynes, *Chem. Commun.*, 2011, **47**, 532–534.
- 29 F. F. Cheng, J. J. Zhang, F. Xu, L. H. Hu, E. S. Abdel-Halim and J. J. Zhu, *J. Biomed. Nanotechnol.*, 2013, **9**, 1155–1163.
- 30 Z. H. Zhu, D. Y. Li, Y. N. Li, X. G. Yang and W. S. Pan, *RSC Adv.*, 2017, **7**, 23942–23953.
- 31 X. H. Liu, C. H. Gao, J. H. Gu, Y. F. Jiang, X. L. Yang, S. Y. Li, W. Gao, T. An, H. Q. Duan, J. W. Fu, Y. S. Wang and X. Y. Yang, *ACS Appl. Mater. Interfaces*, 2016, **8**, 27622–27631.
- 32 Z. Tian, X. Yao, K. Ma, X. Niu, J. Grothe, Q. Xu, L. Liu, S. Kaskel and Y. Zhu, *ACS Omega*, 2017, **2**, 1249–1258.
- 33 L. F. Ren, X. J. Liu, Q. Wang, L. J. Zhang, G. Y. Deng, F. Zhou and J. Lu, *Dalton Trans.*, 2017, **46**, 2204–2213.
- 34 W. X. Mao, X. J. Lin, W. Zhang, Z. X. Chi, R. W. Lyu, A. M. Cao and L. J. Wan, *Chem. Commun.*, 2016, **52**, 7122–7125.
- 35 Y. M. Hu, J. D. Chen, T. T. Fan, Y. J. Zhang, Y. Zhao, X. T. Shi and Q. Q. Zhang, *Colloids Surf., B*, 2017, **157**, 93–100.
- 36 C. C. Zheng, Y. Wang, S. Z. F. Phua, W. Q. Lim and Y. L. Zhao, *ACS Biomater. Sci. Eng.*, 2017, **3**, 2223–2229.
- 37 S. G. Wang, Y. L. Wu, R. Guo, Y. P. Huang, S. H. Wen, M. W. Shen, J. H. Wang and X. Y. Shi, *Langmuir*, 2013, **29**, 5030–5036.
- 38 L. L. Dai, J. J. Liu, Z. Luo, M. H. Li and K. Y. Cai, *J. Mater. Chem. B*, 2016, **4**, 6758–6772.
- 39 K. A. Iczkowski, *Am. J. Transl. Res.*, 2011, **3**, 1–7.
- 40 P. Kesharwani, S. Banerjee, S. Padhye, F. H. Sarkar and A. K. Iyer, *Biomacromolecules*, 2015, **16**, 3042–3053.
- 41 F. Zhao, Y. Zhao, Y. Liu, X. L. Chang, C. Y. Chen and Y. L. Zhao, *Small*, 2011, **7**, 1322–1337.
- 42 W. Feng, W. Nie, C. L. He, X. J. Zhou, L. Chen, K. X. Qiu, W. Z. Wang and Z. Q. Yin, *ACS Appl. Mater. Interfaces*, 2014, **6**, 8447–8460.
- 43 M. H. Yu, S. Jambhrunkar, P. Thorn, J. Z. Chen, W. Y. Gu and C. Z. Yu, *Nanoscale*, 2013, **5**, 178–183.
- 44 K. Y. Ju, J. W. Lee, G. H. Im, S. Lee, J. Pyo, S. B. Park, J. H. Lee and J. K. Lee, *Biomacromolecules*, 2013, **14**, 3491–3497.
- 45 K. Y. Ju, S. Lee, J. Pyo, J. Choo and J. K. Lee, *Small*, 2015, **11**, 84–89.

